Inorganic Chemistry

Article

pubs.acs.org/IC

Strong Solvent-Dependent Preference of Δ and Λ Stereoisomers of a Tris(diamine)nickel(II) Complex Revealed by Vibrational Circular Dichroism Spectroscopy

Christian Merten,*[,†,‡] Robert McDonald,[†] and Yunjie Xu*[,†]

[†]Department of Chemistry, University of Alberta, Edmonton T6G2G2, Canada

[‡]Fakultät für Chemie und Biochemie, Ruhr-Universität Bochum, 44801 Bochum, Germany

Supporting Information

ABSTRACT: In the present study, we use vibrational circular dichroism (VCD) spectroscopy to investigate the metal-centered Δ and Λ chirality of a tris(diamine)nickel(II) complex. Chiral diphenylethylenediamine is chosen as the ligand, which puts the Δ and Λ isomers of the complex in a diastereomeric relationship. X-ray crystallography indicates an equal preference of both stereoisomers in the solid state. This equal preference is also supported by the related density functional theory calculations. A comparison between the experimental and calculated VCD spectra also proves the existence of both isomers in an acetonitrile solution. However, a significant shift of the equilibrium toward the Λ diastereomer is found for the complex in dimethyl sulfoxide. This solvent-induced preference for a particular absolute configuration is hypothesized to arise from a stronger and more effective solvation of the Λ isomer. The observation that the solvent can significantly influence and shift an equilibrium between two diastereomeric forms is expected to have important implications on structural analysis and on how reaction mechanisms are rationalized.

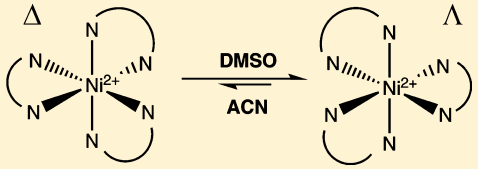

INTRODUCTION

Chiral transition-metal complexes are frequently used as catalysts in asymmetric synthesis. Some of the very well-known examples include complexes of the bidentate diphosphine ligand (1,1′-binaphthalene)-2,2′-diylbis-(diphenylphosphine) (BINAP) and its derivatives, which are used in hydrogenation reactions,[1−3] and complexes of Schiff bases like Jacobson's salen catalysts for epoxidation reactions.[4,5] The structures of metal complexes are typically determined by single-crystal X-ray analysis and, if applicable, with NMR studies. While single-crystal analysis yields the absolute configuration of the chiral ligands and the metal center, as well as the preferred conformation in the solid state, solvent-driven dynamical aspects cannot be investigated. NMR spectroscopy and especially 2D NMR techniques, on the other hand, can capture certain solvent effects, but they are insensitive to chirality without the addition of chiral auxiliaries. From measurements of the electronic circular dichroism (ECD), general information on the chirality of metal complexes can be derived. The conformational sensitivity of ECD spectroscopy, however, is limited.

For studies on chiral transition-metal complexes, vibrational circular dichroism (VCD) spectroscopy has become a powerful alternative to ECD because of its high sensitivity to chirality and to conformational preferences. VCD spectroscopy is today frequently applied to the determination of absolute configurations. Moreover, it has been shown to be a leading tool for the investigation of conformational preferences and solvent effects for a variety of materials.[6,7] Such applications range from conformational studies of biomolecules such as peptides and sugars to studies on solvent-dependent self-aggregation[8−10] and chirality transfer,[11−13] and studies on polymers[14,15] and nanoparticles.[16] In the field of chiral metal complexes, only a few studies have been carried out, which can mostly be attributed to the high computational costs of the density functional theory (DFT)-based VCD spectral calculations of metal complexes. Studies on small systems typically include calculations, for instance, for Schiff base complexes,[17,18] the well-known BINAP systems,[19] complexes with amino acids,[20] or complexes with π-donor ligands.[21,22] For larger systems, VCD has been used only to provide evidence for the formation of large chiral structures, without detailed interpretation of the spectral features.[23] More systematic studies on the spectrum−structure relationships have been carried out by Sato et al. on β-diketonato complexes[24−26] and by Merten et al. on complexes with chiral diamine ligands.[27,28] In the latter studies, it was shown that the VCD pattern of the NH_2 bending modes can be correlated to the coordination number of a diamine complex and used as an indicator for the Δ and Λ configurations around the metal center in tris(diamine) complexes.[27]

In an effort to further generalize the spectrum−structure correlations for metal complexes of chiral diamines, we investigate in the present work the VCD spectra of two new transition-metal complexes of copper(II) and nickel(II) as bis- and tris-coordinated metal centers with diphenylethylenediamine (dipen) as the chiral ligand (cf. Scheme 1). Dipen has been chosen as the chiral ligand for this model study because of

Received: January 7, 2014
Published: March 6, 2014

   dx.doi.org/10.1021/ic4031766 | Inorg. Chem. 2014, 53, 3177−3182

Scheme 1. Structure of the Ligand and the Target Metal Complexes

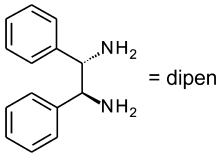

1 $[Cu(dipen)_2(ClO_4)_2]$

2 $[Ni(dipen)_3](ClO_4)_2 \cdot H_2O$

its conformational flexibility and because it is already used as the ligand in asymmetric catalysts such as $RuCl_2[(S)\text{-}(XylBINAP)][(S,S)\text{-dipen}]$.[29] Starting with $[Cu(dipen)_2(ClO_4)_2]$ (**1**), we first establish the appropriate procedure for simulating VCD spectra and performing VCD spectral analysis. Then, on the basis of a comparison of the experimental and theoretical spectra, we show that, depending on the solvent environment, $[Ni(dipen)_3(ClO_4)_2]\cdot H_2O$ (**2**) takes on different preferred configurations at the metal center, i.e., different diastereomeric absolute configurations. This unexpected finding, that is, the choice of the solvent controls diastereomeric preferences, has important implications on structural analysis and on how reaction mechanisms are rationalized.

MATERIALS AND METHODS

Materials. Both enantiomers of dipen were obtained from Alfa Aesar, while all other chemicals were purchased from Sigma Aldrich (Canada). All chemicals were used without further purification.

Synthesis of $[Cu(dipen)_2(ClO_4)_2]$ (1). To a solution of 1 equiv of $Cu(ClO_4)_2\cdot 6H_2O$ in methanol was added a solution of 2 equiv of (*S,S*)- or (*R,R*)-dipen in methanol. After the solid purple product that precipitated upon the addition of the diamine solution was filtered, single crystals were obtained from acetone/methanol by slow evaporation of the solvent. Yield: >95%. Elem anal. Calcd for $C_{28}H_{32}N_4O_8Cl_2Cu$: C, 48.95; H, 4.69; N, 8.15. Found: C, 48.99; H, 4.71; N, 8.14. Optical rotation of (*S,S*)-**1**: $[\alpha]^{298\ K}_D = -179.18°$ (c = 1.027, DMSO) and $[\alpha]^{298\ K}_D = -167.68°$ (c = 1.014, ACN).

Synthesis of $[Ni(dipen)_3(ClO_4)_2]\cdot H_2O$ (2). Similar to the synthesis of **1**, $Ni(ClO_4)_2\cdot 6H_2O$ and (*S,S*)- or (*R,R*)-dipen were mixed in methanol in a 1:3 ratio. After evaporation of the solvent, the purple solid was washed several times with diethyl ether. Crystals suitable for X-ray analysis were grown from a saturated solution of (*S,S*)-**2** in dimethyl sulfoxide (DMSO). Yield: >95%. Elem anal. Calcd for $C_{42}H_{50}N_6O_9Cl_2Ni$: C, 55.28; H, 5.52; N, 9.21. Found: C, 55.19; H, 5.43; N, 9.08. Optical rotation of (*R,R*)-**2**: $[\alpha]^{298\ K}_D = -73.18°$ (c = 1.031, DMSO) and $[\alpha]^{298\ K}_D = -57.02°$ (c = 1.045, ACN).

X-ray Crystallography. Single-crystal X-ray diffraction measurements of **1** and **2** were carried with Mo Kα radiation (λ = 0.71073 Å) on a Bruker PLATFORM diffractometer equipped with an APEX II CCD area detector with the crystal cooled to −100 °C. The data were corrected for absorption by Gaussian integration from indexing of the crystal faces.[30] Structures were solved using the Patterson search/structure expansion facilities within the *DIRDIF-2008* program system[31] (**1**) or using intrinsic phasing (*SHELXT*;[32] **2**). Structure refinement was accomplished using *SHELXL-97*.[32] Hydrogen atoms were assigned positions based on the sp^2 or sp^3 hybridization geometries of their attached carbon and nitrogen atoms.

IR and VCD Spectroscopy. The IR and VCD spectra were recorded in the fingerprint region (1800−850 cm^{-1}) on a Bruker Vertex 70 FT-IR spectrometer equipped with a Bruker PMA 50 module for VCD measurements. The samples were held in a demountable BaF_2 cell with 100 μm path length. For the VCD spectra, a minimum of 20000 scans was averaged. The concentration of the metal complexes in DMSO-d_6 and acetonitrile (ACN)-d_3 was 130 mg/mL. The spectral range from 1140 to 1000 cm^{-1} was cut out in all experimental spectra because of interference with absorbance bands of the solvent and the perchlorate ion.

UV and ECD Spectroscopy. The UV and ECD spectra of **2** were measured at 1 cm path length (c = 22 mM) in the spectral range from 300 to 700 nm using an HP 8453 UV−vis instrument and an Olis DSM 17 CD spectrophotometer, respectively.

Computational Details. Geometry optimizations and IR and VCD spectral calculations were performed in the DFT framework at the B3LYP/6-31+G(2d,p) level of theory using *Gaussian09*, version D.01.[33] The vibrational spectra were calculated for the (*R,R*) enantiomers in the gas phase and with the integral equation formalism version of the polarizable continuum model (IEFPCM)[34,35] for DMSO. Vibrational line broadening was taken into account by assigning a Lorentzian band shape with a half-width at half-height of 6 cm^{-1} to the calculated dipole and rotational strength. The calculated wavenumbers were scaled by a factor of 0.98 for a better comparison with the experimental data.

RESULTS AND DISCUSSION

Bis-complex 1. The crystal structure of **1** is shown in Figure 1. In the solid state, two dipen ligands chelate the copper

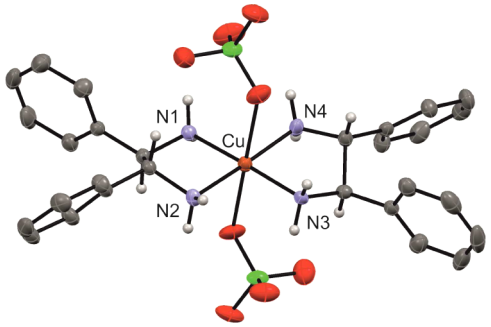

Figure 1. Crystal structure of (*R,R*)-**1**. Non-hydrogen atoms are represented by Gaussian ellipsoids at the 50% probability level. Hydrogen atoms are shown with arbitrarily small thermal parameters except for the phenyl-group hydrogen atoms, which are not shown.

ion, forming a square-planar geometry. Additionally, two oxygen atoms of two perchlorate ions complete the coordination sphere on the axial positions. The interatomic Cu−N and Cu−O distances are in good agreement with distances reported for other diamine complexes of copper(II), e.g., the complex with *trans*-1,2-diaminocyclohexane (chxn).[36] In the crystal structure, the chiral dipen ligand adopts a λ conformation, with the N−C−C−N torsion angle being near −60°. However, the two N−C−C−N torsion angles (see below) in the crystal differ by ∼5°, so that **1** does not retain a perfect square-planar geometry in the solid state; the dihedral angle between the planes defined by Cu−N1−N2 and Cu−N3−N4 is 4.65(19)°.

In solution, it is expected that the perchlorate ions become solvated and hence separated from the metal center. Therefore, for conformational analysis and calculations of IR and VCD spectra, only the cation $[Cu(dipen)_2]^{2+}$ was considered. It can also be assumed that the cation in solution would feature a higher symmetry than that in the solid. For the closely related $[Cu(chxn)_2(ClO_4)_2]$ complex, these assumptions had been shown to be reasonable.[27] Furthermore, the dipen ligand can theoretically also adopt a δ conformation, with the N−C−C−N angle being about +60°. Therefore, three possible structures of **1** with $\lambda\lambda$, $\lambda\delta$, and $\delta\delta$ conformations of the two dipen ligands were all considered in the conformational analysis.

Table 1 summarizes the gas-phase energies and corresponding Boltzmann populations of these three conformers obtained at the B3LYP/6-31+G(2d,p) level of theory. The optimized

dx.doi.org/10.1021/ic4031766 | Inorg. Chem. 2014, 53, 3177−3182

Table 1. Relative Energies ΔE and ΔG (in kcal/mol) at Room Temperature and Corresponding Boltzmann Populations (in %) of 1 in the Gas Phase Calculated at the B3LYP/6-31+G(2d,p) Level of Theory

conformer	ΔE^a	ΔG^b	pop-ΔE	pop-ΔG
$\lambda\lambda$	0.00	0.00	98.8	99.9
$\lambda\delta$	2.26	2.47	2.2	1.5
$\delta\delta$	6.36	7.15	0.0	0.0

[a] ΔE is referenced to the zero-point-energy-corrected energy of conformer $\lambda\lambda$ at $-2944.731799E_h$. [b] ΔG is referenced to the Gibbs energy of conformer $\lambda\lambda$ at $-2944.797544E_h$.

structures are shown in the Supporting Information (Figure S1). The computed energy differences clearly indicate that the $\lambda\lambda$ isomer, the same observed in the solid, is strongly favored over the $\lambda\delta$ and $\delta\delta$ isomers. Further calculations, with a larger basis set [6-311++G(2d,p)] and with the inclusion of implicit solvation using the IEFPCM,[34,35] yielded similar results, which are summarized in the Supporting Information (Table S1).

The experimental IR and VCD spectra of both enantiomers of **1** measured in DMSO-d_6 are presented in Figure 2. Spectra

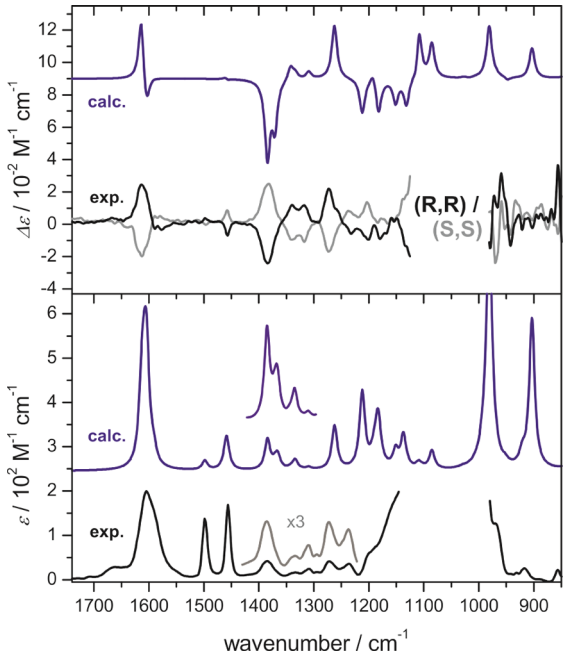

Figure 2. Experimental VCD and IR spectra of **1** in DMSO-d_6 compared to the corresponding calculated spectra for (*R*,*R*)-[Cu(dipen)$_2$]$^{2+}$ in the gas phase. The results of the IEFPCM calculations are shown in the Supporting Information (Figure S3).

obtained from ACN solutions are very similar with just minor band shifts. A comparison is provided in the Supporting Information (Figure S2). In general, the VCD spectra of the pair of enantiomers show very good mirror-image quality and many very strong bands. The most important band corresponds to the NH_2 bending mode, which is found at ~1600 cm^{-1}. It shows a ± pattern for the (*R*,*R*) enantiomer (read from higher to lower wavenumbers) with a slightly weaker negative component than was observed for (*R*,*R*)-[Cu(chxn)$_2$(ClO$_4$)$_2$].[27] The spectral range from 1150 to 980 cm^{-1} was left out because of interferences from bands of the solvent and the anion.

The calculated population-weighted spectra shown in Figure 2 correspond mainly to the single-conformer spectra of the $\lambda\lambda$ isomer because conformational analysis showed a clear preference for this conformer. The agreement with the experimental spectra is quite good, and all of the main spectral features such as the couplet of the NH_2 bending mode are reproduced. The spectra calculated in the IEFPCM framework show no obvious improvement, and we therefore focus on the gas-phase calculations as the model chemistry of choice.

Tris-complex 2. Figure 3 shows the crystal structure of complex (*S*,*S*)-**2** as obtained for crystals grown from DMSO. It

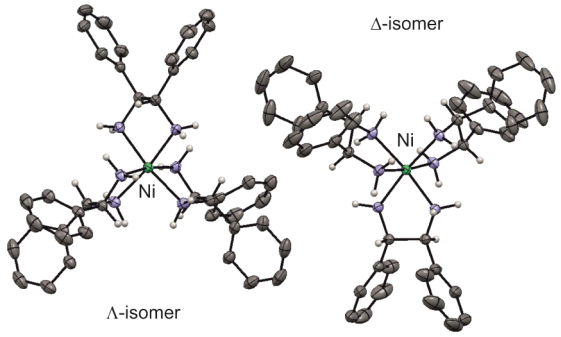

Figure 3. Crystal structure of (*S*,*S*)-[Ni(dipen)$_3$]$^{2+}$. Non-hydrogen atoms are represented by Gaussian ellipsoids at the 50% probability level. Hydrogen atoms are shown with arbitrarily small thermal parameters except for the phenyl-group hydrogen atoms, which are not shown. The perchlorate ions and crystallization solvent are also omitted.

was found to adopt the $\Delta(\delta\delta\delta)$ and $\Lambda(\delta\delta\delta)$ configuration around the metal center with equal preference within a unit cell. Hence, independent of the chirality of the diamine ligand, both configurations around the metal center are adopted with the same preference. In contrast, the related complex of (*R*,*R*)-[Ni(chxn)$_3$]Br$_2$·3H$_2$O was found to prefer solely the $\Delta(\lambda\lambda\lambda)$ form in the solid state.[37]

IR and VCD spectra of both enantiomers of **2** were measured in two solvents, i.e., DMSO-d_6 and ACN-d_3 (Figure 4). VCD spectra of the enantiomeric pair in each solution show again very good mirror-image quality featuring several strong bands. However, when the two sets of spectra taken in the two different solvents are compared, significantly different VCD patterns are found for the NH_2 bending mode around 1600 cm^{-1}. In the case of ACN as the solvent, the NH_2 bending mode of the (*R*,*R*) enantiomer features a ∓ pattern (again read from higher to lower wavenumbers). In DMSO, the VCD bands for the NH_2 bending mode are weaker and appear as two positive bands. In contrast, a ∓ pattern was observed for the related complex (*R*,*R*)-[Ni(chxn)$_3$](ClO$_4$)$_2$·H$_2$O in both solvents. Further minor differences can be observed, for instance, in the range between 1350 and 1300 cm^{-1} or for the intensity ratio of the VCD bands between 1250 and 1200 cm^{-1}. In the IR spectra, differences are much less obvious: while the NH_2 bending mode is centered at 1604 cm^{-1} in the spectrum taken in DMSO, a strong band at 1594 cm^{-1} is dominating the ACN spectrum.

Both the X-ray results and conformational analysis of **1** indicated a negligible amount of δ conformation of the dipen ligand. Therefore, only the $\Delta(\lambda\lambda\lambda)$ and $\Lambda(\lambda\lambda\lambda)$ isomers were considered in the conformational analysis of **2**. The gas-phase calculations predict a preference of the Δ form over the Λ form

dx.doi.org/10.1021/ic4031766 | Inorg. Chem. 2014, 53, 3177−3182

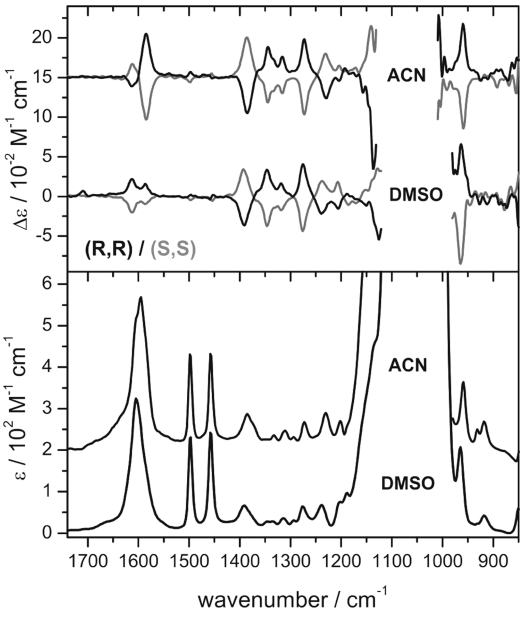

Figure 4. Experimental VCD and IR spectra of **2** in ACN-d_3 (top) and DMSO-d_6, (bottom).

of only ΔE = 0.04 kcal/mol and ΔG = 0.38 kcal/mol. Hence, the DFT calculations reflect the equal preference of both Δ and Λ isomers found in the solid state.

Figure 5 shows the predicted gas-phase spectra of both Δ and Λ forms of (*R*,*R*)-$[Ni(dipen)_3]^{2+}$ in comparison with the

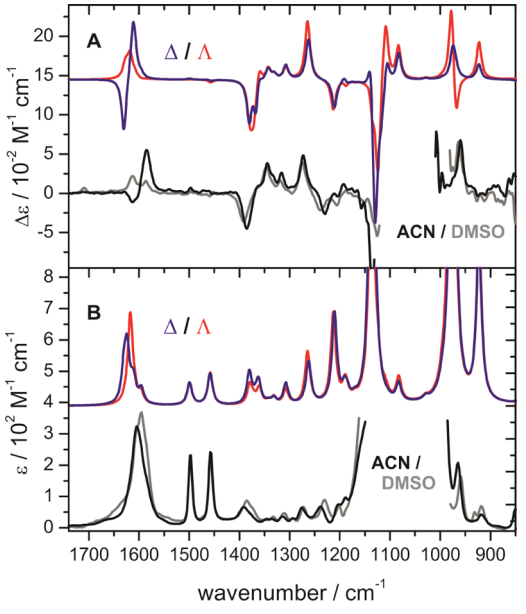

Figure 5. (a) Experimental VCD spectra of (*R*,*R*)-**2** in ACN-d_3 (black) and DMSO-d_6 (gray) compared to the single conformer spectra of (*R*,*R*)-$[Ni(dipen)_3]^{2+}$ in its two diastereomeric configurations (Δ in blue and Λ in red). (b) Same comparison for the corresponding IR spectra.

experimental data of the (*R*,*R*) enantiomer of **2** obtained in both solvents. The predicted IR spectra of both isomers are very similar, so are the VCD spectral features in the range from 1500 to 1200 cm^{-1}. The only major difference in the theoretical spectra of the Δ and Λ forms of (*R*,*R*)-$[Ni(dipen)_3]^{2+}$ can be found for the NH_2 bending mode between 1675 and 1575 cm^{-1} and below 1200 cm^{-1}. Unfortunately, the latter region is partially obscured in the experiment by interference of the solvent and the anion bands, and its quality is less desirable for the detailed interpretation of the spectra. The experimentally observed difference in the NH_2 bending mode, on the other hand, can be explained based on these calculations. It is predicted to show a ∓ pattern for the Δ isomer and a solely positive pattern for the Λ isomer. These patterns are in agreement with our previous studies on 1,2-diamine-based metal complexes in which the correlation between the NH_2 bending pattern and the absolute configuration of the central metal ions was established.[27,28]

By a comparison of the experimental and theoretical spectra, complex **2** is shown to preferably adopt the Λ form in DMSO solutions. In ACN, the negative and positive components feature a ratio of about 1:3 in the experiment. This is best explained by an equal mixture of the Δ and Λ forms, just as predicted by the theoretical Boltzmann's population factors.

Different absolute configurations around the metal center should also result in different ECD bands for the metal d−d transitions because the Δ and Λ forms about the metal center would have mirror-imaged ECD spectra if there were no additional ligand chirality.[38] Some differences in the ECD spectra for isomers Δ(λλλ) and Λ(λλλ) of **2**, which have opposite chirality at the metal center, would be expected even though they do possess ligand chirality and are diastereomers to each other in the current case. Therefore, the ECD of **2** was measured as further experimental support of the interpretation: solvent-driven absolute configuration preference. Figure 6

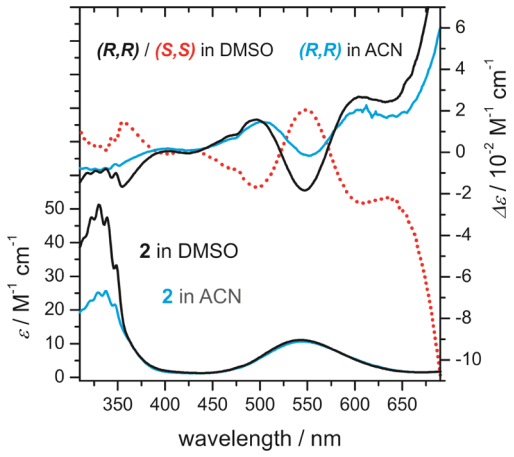

Figure 6. Comparison of the experimental UV and ECD spectra of **2** in DMSO and ACN.

shows the experimental ECD spectra of **2** obtained in DMSO-d_6 and ACN-d_3. The broad d−d transition centered at 540 nm features a clear ±/+ pattern for the (*R*,*R*) enantiomer in DMSO, while the negative component is much weaker in ACN. These changes might also indicate a solvent dependence, although it could easily be overlooked because the spectral differences are less obvious than those in the VCD. Generalizing a correlation between the experimental ECD pattern and configurations at the metal center is, however, difficult. It is also of little use for routine structural analysis because the nature of the metal center, i.e., its electron configuration, has a significant influence on the transition wavelength and ECD pattern. For VCD spectroscopy, on the other hand, only the structural aspect of the Δ or Λ

dx.doi.org/10.1021/ic4031766 | Inorg. Chem. 2014, 53, 3177−3182

configuration matters but not the electronic configuration. This, in turn, highlights the power of VCD spectroscopy in these kinds of studies.

The preference of the Λ isomer is DMSO is likely to be related to the hydrogen-bonding network formed between DMSO solvent molecules and amine hydrogen atoms. Attempts have been made to determine the number of DMSO molecules surrounding the Δ and Λ forms of $[Ni(dipen)_3]^{2+}$ by systematically placing DMSO molecules around the optimized geometries. For steric reasons, the Λ isomer can be solvated with six DMSO molecules while only five can be placed around the Δ form (see the schematic drawings in Figures S4−S7 in the Supporting Information). This different number of solvent molecules may lead to qualitatively different solvation energies and therefore the preference of the Λ isomer. Detailed theoretical modeling of the associated solvation, however, requires a significant amount of computational resources and is out of the scope of the current study.

CONCLUSIONS

In a summary of the present work, a VCD spectroscopic study of two metal complexes with the chiral diamine dipen as the ligand was carried out. It could be shown that the dipen ligand preferably adopts the λ conformation in both the bis- and tris-complexes studied here. For the tris-nickel(II) complex, an equal mixture of Δ and Λ isomers was identified in the solid-state structure. While the parent IR spectra of the tris-nickel(II) complex in DMSO and ACN look more or less the same, the corresponding VCD spectra show significant solvent-dependent features for the NH_2 bending mode. The observation indicates a solvent-induced absolute configuration change, i.e., a strong preference of the Λ form in DMSO and an equal mixture of the Δ and Λ isomers in ACN.

The results of this study have significant implications on the experimental and theoretical aspects of chiral transition-metal chemistry,[39−41] such as the development of asymmetric catalysts. Solvent-driven absolute configuration changes of paramagnetic metal complexes like the one described in this study cannot be predicted or inferred from NMR studies or solid-state structures. Therefore, more emphasis should be placed on chiroptical spectroscopic studies of chiral metal complexes in order to uncover and better understand solvent-dependent structural changes in general. Future systematic investigations on other common ligand binding schemes such as Schiff bases and salen-based complexes would be valuable in order to firmly establish empirical relations between absolute configurations and their corresponding VCD spectral patterns and to identify solvent-driven structural changes.

ASSOCIATED CONTENT

Supporting Information

Crystallographic information, including a CIF file, for **1** and **2**, additional computational and experimental data on **1**, structures of solvated **2**, and Cartesian coordinates of the optimized structures of **1** and **2**. This material is available free of charge via the Internet at http://pubs.acs.org.

AUTHOR INFORMATION

Corresponding Authors

*E-mail: christian.merten@ruhr-uni-bochum.de.
*E-mail: yunjie.xu@ualberta.ca.

Notes

The authors declare no competing financial interest.

ACKNOWLEDGMENTS

The authors thank Wayne Moffat and the members of the Analytical Instrumentation Lab of the University of Alberta for carrying out the elemental analysis and ECD measurements. C.M. acknowledges financial support by the Alexander von Humboldt Foundation for a Feodor Lynen Postdoctoral fellowship and the Fonds der chemischen Industrie for a Liebig fellowship. This research was supported by the University of Alberta, the Natural Sciences and Engineering Research Council of Canada, and the Canada Research Chairs Program, as well as the Deutsche Forschungsgemeinschaft through the Cluster of Excellence RESOLV (EXC 1069). We also gratefully acknowledge access to the computing facilities provided by the Western Canada Research Grid (Westgrid).

REFERENCES

(1) Mashima, K.; Kusano, K.-h.; Sato, N.; Matsumura, Y.-i.; Nozaki, K.; Kumobayashi, H.; Sayo, N.; Hori, Y.; Ishizaki, T. *J. Org. Chem.* **1994**, *59*, 3064−3076.
(2) Kitamura, M.; Ohkuma, T.; Inoue, S.; Sayo, N.; Kumobayashi, H.; Akutagawa, S.; Ohta, T.; Takaya, H.; Noyori, R. *J. Am. Chem. Soc.* **1988**, *110*, 629−631.
(3) Sandoval, C. A.; Ohkuma, T.; Muñiz, K.; Noyori, R. *J. Am. Chem. Soc.* **2003**, *125*, 13490−13503.
(4) Zhang, W.; Loebach, J. L.; Wilson, S. R.; Jacobsen, E. N. *J. Am. Chem. Soc.* **1990**, *112*, 2801−2803.
(5) Jacobsen, E. N.; Zhang, W.; Muci, A. R.; Ecker, J. R.; Deng, L. *J. Am. Chem. Soc.* **1991**, *113*, 7063−7064.
(6) Yang, G.; Xu, Y. *Top. Curr. Chem.* **2011**, *298*, 189−236.
(7) Sadlej, J.; Dobrowolski, J. C.; Rode, J. E. *Chem. Soc. Rev.* **2010**, *39*, 1478−1488.
(8) Losada, M.; Tran, H.; Xu, Y. *J. Chem. Phys.* **2008**, *128*, 014508.
(9) Liu, Y.; Yang, G.; Losada, M.; Xu, Y. *J. Chem. Phys.* **2010**, *132*, 234513.
(10) Merten, C.; Amkreutz, M.; Hartwig, A. *Phys. Chem. Chem. Phys.* **2010**, *12*, 11635−11641.
(11) Losada, M.; Xu, Y. *Phys. Chem. Chem. Phys.* **2007**, *9*, 3127−3135.
(12) Yang, G.; Xu, Y. *J. Chem. Phys.* **2009**, *130*, 164506.
(13) Merten, C.; Xu, Y. *Angew. Chem., Int. Ed.* **2013**, *52*, 2073−2076.
(14) Tang, H.-Z.; Garland, E. R.; Novak, B. M.; He, J.; Polavarapu, P. L.; Sun, F. C.; Sheiko, S. S. *Macromolecules* **2007**, *40*, 3575−3580.
(15) Merten, C.; Hartwig, A. *Macromolecules* **2010**, *43*, 8373−8378.
(16) Gautier, C.; Bürgi, T. *J. Phys. Chem. C* **2010**, *114*, 15897−15902.
(17) Chamayou, A.-C.; Lüdeke, S.; Brecht, V.; Freedman, T. B.; Nafie, L. A.; Janiak, C. *Inorg. Chem.* **2011**, *50*, 11363−11374.
(18) Sato, H.; Mori, Y.; Yamagishi, A. *Dalton Trans.* **2013**, *42*, 6873−6878.
(19) Dezhahang, Z.; Merten, C.; Poopari, M. R.; Xu, Y. *Dalton Trans.* **2012**, *41*, 10817−10824.
(20) Szilvagyi, G.; Brem, B.; Bati, G.; Tolgyesi, L.; Hollosi, M.; Vass, E. *Dalton Trans.* **2013**, *42*, 13137−13144.
(21) Merten, C.; Amkreutz, M.; Hartwig, A. *J. Mol. Struct.* **2010**, *970*, 101−105.
(22) Stephens, P. J.; Devlin, F. J.; Villani, C.; Gasparrini, F.; Mortera, S. L. *Inorg. Chim. Acta* **2008**, *361*, 987−999.
(23) Jahier, C.; Cantuel, M.; McClenaghan, N. D.; Buffeteau, T.; Cavagnat, D.; Agbossou, F.; Carraro, M.; Bonchio, M.; Nlate, S. *Chem.—Eur. J.* **2009**, *15*, 8703−8708.
(24) Sato, H.; Taniguchi, T.; Monde, K.; Nishimura, S.-I.; Yamagishi, A. *Chem. Lett.* **2006**, *35*, 364−365.
(25) Sato, H.; Taniguchi, T.; Nakahashi, A.; Monde, K.; Yamagishi, A. *Inorg. Chem.* **2007**, *46*, 6755−6766.
(26) Sato, H.; Yamagishi, A. *Int. J. Mol. Sci.* **2013**, *14*, 964−978.

(27) Merten, C.; Hiller, K.; Xu, Y. *Phys. Chem. Chem. Phys.* **2012**, *14*, 12884−12891.
(28) Merten, C.; Xu, Y. *Dalton Trans.* **2013**, *42*, 10572−10578.
(29) Ohkuma, T.; Doucet, H.; Pham, T.; Mikami, K.; Korenaga, T.; Terada, M.; Noyori, R. *J. Am. Chem. Soc.* **1998**, *120*, 1086−1087.
(30) Programs for diffractometer operation, data collection, data reduction, and absorption correction were those supplied by Bruker.
(31) Beurskens, P. T.; Beurskens, G.; Gelder, R. d.; Smits, J. M. M.; Garcia-Granda, S.; Gould, R. O. *DIRDIF-2008*; Crystallography Laboratory, Radboud University: Nijmegen, The Netherlands, 2008.
(32) Sheldrick, G. *Acta Crystallogr., Sect. A* **2008**, *64*, 112−122.
(33) Frisch, M. J.; Trucks, G. W.; Schlegel, H. B.; Scuseria, G. E.; Robb, M. A.; Cheeseman, J. R.; Scalmani, G.; Barone, V.; Mennucci, B.; Petersson, G. A.; Nakatsuji, H.; Caricato, M.; Li, X.; Hratchian, H. P.; Izmaylov, A. F.; Bloino, J.; Zheng, G.; Sonnenberg, J. L.; Hada, M.; Ehara, M.; Toyota, K.; Fukuda, R.; Hasegawa, J.; Ishida, M.; Nakajima, T.; Honda, Y.; Kitao, O.; Nakai, H.; Vreven, T.; Montgomery, J. A., Jr.; Peralta, J. E.; Ogliaro, F.; Bearpark, M.; Heyd, J. J.; Brothers, E.; Kudin, K. N.; Staroverov, V. N.; Keith, T.; Kobayashi, R.; Normand, J.; Raghavachari, K.; Rendell, A.; Burant, J. C.; Iyengar, S. S.; Tomasi, J.; Cossi, M.; Rega, N.; Millam, J. M.; Klene, M.; Knox, J. E.; Cross, J. B.; Bakken, V.; Adamo, C.; Jaramillo, J.; Gomperts, R.; Stratmann, R. E.; Yazyev, O.; Austin, A. J.; Cammi, R.; Pomelli, C.; Ochterski, J. W.; Martin, R. L.; Morokuma, K.; Zakrzewski, V. G.; Voth, G. A.; Salvador, P.; Dannenberg, J. J.; Dapprich, S.; Daniels, A. D.; Farkas, O.; Foresman, J. B.; Ortiz, J. V.; Cioslowski, J.; Fox, D. J. *Gaussian09*, version D.01; Gaussian, Inc.: Wallingford, CT, 2013.
(34) Mennucci, B.; Cappelli, C.; Cammi, R.; Tomasi, J. *Chirality* **2011**, *23*, 717−729.
(35) Tomasi, J.; Mennucci, B.; Cammi, R. *Chem. Rev.* **2005**, *105*, 2999−3094.
(36) Pariya, C.; Panneerselvan, K.; Chung, C.-S.; Lub, T.-H. *Polyhedron* **1998**, *17*, 2555−2561.
(37) Ishida, K.; Tanase, T.; Takahashi, T.; Sato, Y.; Yano, S.; Hidai, M.; Kobayashi, K.; Sakurai, T. *Acta Crystallogr., Sect. C* **1988**, *44*, 83−85.
(38) Telfer, S. G.; McLean, T. M.; Waterland, M. R. *Dalton Trans.* **2011**, *40*, 3097−3108.
(39) Crassous, J. *Chem. Soc. Rev.* **2009**, *38*, 830−845.
(40) Crassous, J. *Chem. Commun.* **2012**, *48*, 9687−9695.
(41) Meggers, E. *Eur. J. Inorg. Chem.* **2011**, *2011*, 2911−2926.